Bio-chemo-hydro-mechanical finite element modeling of microbially induced calcite precipitation for optimal treatment design

Alireza Azizi[1], *Kamelia* Atefi-Monfared[1*]

[1] Department of Civil Engineering, Lassonde School of Engineering, York University, Toronto, Ontario, Canada

Abstract. To overcome the limitations associated with conventional cement-based soil stabilization methods, Microbially Induced Calcite Precipitation (MICP) has emerged as a sustainable alternative for improving soil strength through bio-cementation. Although substantial research has been devoted to understanding, controlling, optimizing, and designing the MICP process, there is still a need for mechanistic yet practical tools that can support the accurate design of treatment strategies and reliably predict treatment performance. This study presents a novel theoretical framework based on a finite element code that couples biological, chemical, hydraulic, and mechanical processes to predict calcium carbonate precipitation and the corresponding improvements observed in both laboratory- and field-scale applications. This study presents a detailed parametric investigation using a fully coupled BCHM finite element model to assess the influence of cyclic treatment on the overall precipitation of calcium carbonate, which is one of the main objectives in sand stabilization. Different cementation solution injection cycles were examined to evaluate how increasing treatment intensity affects calcium carbonate precipitation and its spatial distribution within the column. The results provide valuable information for optimum design of MICP injection strategies.

1 Introduction

Microbially Induced Calcite Precipitation (MICP) is a sustainable ground improvement method that relies on bacterial metabolic activity to initiate biochemical reactions that produce calcium carbonate, forming a cement often referred to as bio-cement [1, 2]. In contrast to traditional stabilization approaches, such as the use of Portland cement or chemical resins, MICP generally requires fewer resources and is associated with lower energy consumption, shorter processing demands, and reduced carbon dioxide emissions. Among the microbial pathways used for bio-cementation, urea hydrolysis is widely regarded as the most effective. This pathway requires urease-active bacteria, urea, and a calcium source. During the reaction, urea is hydrolyzed to produce ammonium and carbonate ions, and the carbonate subsequently reacts with calcium ions to form calcium carbonate precipitates, as shown below:

$$CO(NH_2)_2 + 2H_2O \rightarrow 2NH_4^+ + CO_3^{2-}$$
$$Ca^{2+} + CO_3^{2-} \rightarrow CaCO_3$$

The improvement achieved through MICP in porous materials is strongly influenced by how bio-cement is distributed within the medium, which in turn depends on the spatial distribution of bacteria and chemical reactants. MICP is a highly coupled process involving several simultaneous and interrelated mechanisms. The movement of suspended and dissolved species is controlled by advection, dispersion, and diffusion across interacting fluid and solid phases. At the same time, bacterial attachment to soil particles alters the availability of reactive species as biochemical reactions progress. As calcium carbonate precipitates, it either fills pore spaces or creates bridges between particles, modifying pore structure and affecting pore pressure conditions. This mineral accumulation increases the strength and stiffness of the soil skeleton [3, 4], which then influences hydraulic behavior and further changes pore pressure. In addition, crystal growth induces small deformations in the porous matrix, leading to local stress redistribution. Fluid injection also generates pore pressure that contributes to the stress–strain response of the medium, while the resulting deformation feeds back into pore pressure evolution [5]. Because these mechanisms continuously affect one another, reliable modeling of MICP requires a fully coupled perspective.

A considerable number of studies have attempted to model MICP in soils to better represent field conditions and estimate both the amount and spatial distribution of precipitated calcium carbonate [6-9]. However, these models are typically developed under different assumptions, and many treat the process as decoupled or only partially coupled. Frequently adopted simplifications include assuming constant porosity, permeability, stiffness, and bacterial attachment rate during treatment. MICP is an evolving coupled system in which calcium carbonate precipitation progressively changes porosity, permeability, and mechanical

* Corresponding author: catefi@yorku.ca

properties. In addition, the rate of bacterial attachment may vary with injection velocity, highlighting the strongly dynamic nature of the process.

In this study, a finite element model (FEM) was developed to capture the fully coupled nature of the MICP process, and cyclic treatment was incorporated to reflect its common application in practice. The effects of different cementation cycles on both the distribution and the amount of precipitated bio-cement were then investigated.

2 Methodology

A finite element model (FEM) was developed to simulate the coupled biological, chemical, hydraulic, and mechanical (BCHM) processes involved in MICP in a soil column, following the framework proposed by Mehrabi and Atefi-Monfared [5].

The main assumptions are consistent with those reported by Mehrabi and Atefi-Monfared [5]. The porous medium is assumed to be isothermal, fully saturated, homogeneous, and elastic. It is represented by two main phases: a solid phase, composed of soil particles, attached bacteria, and precipitated calcium carbonate, and a fluid phase, consisting of pore water, suspended bacteria, and dissolved chemical species, including urea, calcium, and ammonium. In this formulation, the subscripts "s" and "f" refer to the solid and fluid phases, respectively.

The fluid phase is assumed to be compressible, with no internal generation of pore water. Advective transport is described using Darcy's law, whereas non-advective transport is modeled based on Fick's law. To emphasize the dominant physical mechanisms, adsorption of dissolved species onto solid surfaces and density-driven flow caused by mass density variations are neglected, as their influence is considered minor [8, 9]. For the solid phase, dispersion and diffusion are assumed negligible compared with advection. In addition, the effect of attached bacteria on porosity is ignored, since experimental observations suggest that significant biofilm formation is unlikely over the relatively short durations associated with this process [10].

Biochemical reactions are represented as irreversible first-order kinetic processes. These reactions are controlled by urease activity from both suspended and attached bacteria, together with the concentration of dissolved urea. The effects of secondary variables, such as pH and temperature fluctuations, are assumed to be negligible relative to the influence of bacterial activity and urea availability [10]. Gravitational effects are included in the formulation. The bacterial attachment rate is taken to depend on flow velocity and is assumed to stop once a critical velocity is exceeded. A positive sign convention is adopted for compressive stresses, and the analysis is carried out under plane strain conditions. Internal and external body forces, as well as inertial effects, are neglected, consistent with common assumptions in BCHM formulations.

Because of the strong coupling between pore pressure and deformation, the flow and equilibrium equations of the chemo-hydro-mechanical system are solved simultaneously. The bacterial transport equations are then solved, and their results are incorporated into the transport equations for the chemical species. The output of the chemical transport model is subsequently fed back into the chemo-hydro-mechanical system. Finally, the updated flow properties obtained from the coupled BCHM model are used in the next time step to evaluate bacterial and chemical transport.

At the injection boundary, constant flow rates together with prescribed initial concentrations of bacteria, urea, and calcium ions are imposed. The bottom boundary is mechanically fixed and maintained at zero pore pressure to represent drainage. Initially, the concentrations of all bacteria and chemical species are set to zero, while hydrostatic pore pressure is established throughout the column.

3 Mathematical framework

3.1 Governing equations

In this paper, only the final forms of the derived equations are provided.

3.1.1 Constitutive equation: Stress-Strain

Poroelasticity theory is employed to evaluate the stress–strain behavior of the treated soil. The modified poroelastic formulation, which captures the relationships among the total induced stress, strain, pore pressure, and the volume of precipitated cement, is given in Eq. (1).

$$\sigma_{ij} = 2G\varepsilon_{ij} + \left(K - \frac{2G}{3}\right)\varepsilon_v\delta_{ij} - \alpha p\delta_{ij} - 3K\alpha_c m_c C_c \delta_{ij} \quad (1)$$

In this equation, σ_{ij} denotes the total induced elastic stress tensor; G and K represent the shear and bulk moduli of the medium, respectively; ε_{ij} is the elastic strain tensor; ε_v is the volumetric strain; δ_{ij} is the Kronecker delta; α is Biot's coefficient; and p is the induced pore pressure. The parameter α_c is a constant associated with the volumetric expansion resulting from calcium carbonate crystal growth, m_c is the molar mass of calcium carbonate, and C_c is the calcium carbonate concentration. Accordingly, the term $\alpha_c m_c C_c$ ($\mathrm{m^3/m^3}$) represents the volume of precipitated calcium carbonate per unit volume of the solid matrix. Although α_c may theoretically be estimated as the inverse of the density of calcium carbonate, in practice only a fraction of the precipitated bio-cement contributes to volumetric expansion, since a considerable portion is typically consumed in pore filling.

3.1.2 Constitutive equation: Darcy's law

Darcy's law governs the relationship between fluid flow and pore pressure, as expressed in Eq. (2). In this

equation, q denotes Darcy velocity; v_f and v_s represent the velocities of the fluid and solid phases, respectively. k is the intrinsic permeability; μ is the dynamic viscosity of the fluid; n is the volume fraction of the fluid phase; and g is the gravitational acceleration.

$$q = n\boldsymbol{v_f} = -\frac{k}{\mu}\left(\nabla p + \rho_f \boldsymbol{g}\right) + n\boldsymbol{v_s} \tag{2}$$

3.1.3 Momentum balance

Assuming isothermal equilibrium, the force balance equation is shown in Eqs. (3) to (5).

$$\nabla \cdot \boldsymbol{\sigma} + \rho \boldsymbol{F} = 0 \tag{3}$$

$$\rho = (1-n)\rho_s + (n)\rho_f \tag{4}$$

$$\rho_s = (1-S_c)\rho_g + S_c\rho_c \tag{5}$$

In these expressions, σ represents the total stress, F denotes the total body force, and ρ is the overall density of the porous medium. In addition, ρ_s refers to the density of the solid phase, S_c is the volume fraction of calcium carbonate, and ρ_g and ρ_c denote the densities of the soil grains and calcium carbonate, respectively.

3.1.4 Fluid phase balance

The governing transport equations for dissolved urea, calcium ions, ammonium, and suspended bacteria are correspondingly expressed in Eqs. (6) through (9), respectively.

$$\frac{\partial\left(n(m_u C_u)\right)}{\partial t} = -\nabla \cdot \left(n(m_u C_u)\boldsymbol{v_f}\right) + \nabla \cdot \left(n\boldsymbol{D}\nabla(m_u C_u)\right) - n m_u R_{react} \tag{6}$$

$$\frac{\partial\left(n(m_{Ca^{+2}} C_{Ca^{+2}})\right)}{\partial t} = -\nabla \cdot \left(n(m_{Ca^{+2}} C_{Ca^{+2}})\boldsymbol{v_f}\right) + \nabla \cdot \left(n\boldsymbol{D} \cdot \nabla(m_{Ca^{+2}} C_{Ca^{+2}})\right) - n m_{Ca^{+2}} R_{react} \tag{7}$$

$$\frac{\partial\left(n\left(m_{NH_4^+} C_{NH_4^+}\right)\right)}{\partial t} = -\nabla \cdot \left(n\left(m_{NH_4^+} C_{NH_4^+}\right)\boldsymbol{v_f}\right) + \nabla \cdot \left(n\boldsymbol{D} \cdot \nabla\left(m_{NH_4^+} C_{NH_4^+}\right)\right) + 2n m_{NH_4^+} R_{react} \tag{8}$$

$$\frac{\partial\left(nB_f\right)}{\partial t} = -\nabla \cdot \left(nB_f \boldsymbol{v_f}\right) + \nabla \cdot \left(n\boldsymbol{D}\nabla B_f\right) - nB_f R_{attach} - nB_f R_{decay} \tag{9}$$

In these equations, B_f denotes the concentration of suspended bacteria, while m_u, $m_{Ca^{2+}}$, and $m_{NH_4^+}$ represent the molar masses of dissolved urea, calcium ions, and ammonium ions, respectively. The term R_{react} describes the rate of consumption or production of chemical species per unit pore volume as a result of biochemical reactions. In addition, R_{attach} represents the rate at which suspended bacteria attach to solid grains, whereas R_{decay} denotes the bacterial decay rate, as defined in Eq. (10).

$$R_{react} = R_{max}\frac{C_u}{C_u + K_m}\exp\left(-\frac{t}{t_{max}}\right) \tag{10}$$

In this expression, R_{max} denotes the maximum reaction rate, K_m is the half-saturation constant, t represents the treatment time, and t_{max} is the maximum duration over which the bacteria remain active.

3.1.5 Solid phase balance

By considering the volume fraction of the solid phase as $(1-n)$, the mass balance equations for soil grains, calcium carbonate, and attached bacteria can be expressed in Eqs. (11) to (13), respectively.

$$\frac{\partial\left((1-n)(1-S_c)\rho_g\right)}{\partial t} = -\nabla \cdot \left((1-n)(1-S_c)\rho_g \boldsymbol{v_s}\right) \tag{11}$$

$$\frac{\partial\left((1-n)(S_c)\rho_c\right)}{\partial t} = -\nabla \cdot \left((1-n)(S_c)\rho_c \boldsymbol{v_s}\right) + n m_c R_{react} \tag{12}$$

$$\frac{\partial\left((1-n)B_s\right)}{\partial t} = -\nabla \cdot \left((1-n)B_s \boldsymbol{v_s}\right) + nR_{attach}B_f - (1-n)R_{decay}B_s \tag{13}$$

3.1.6 Permeability

The Kozeny–Carman relationship is employed to describe the dependence of intrinsic permeability on porosity, consistent with its use in previous MICP studies, as given in Eq. (14) [5].

$$k = \left(\frac{(d_{50})^2}{180}\right) \times \left(\frac{n^3}{(1-n)^2}\right) \tag{14}$$

d_{50} is the mean particle size of the sample.

3.1.7 Porosity

Calcium carbonate precipitation leads to a progressive change in porosity, which can be described by Eq. (15). In this equation, the first term accounts for porosity variation caused by hydro-mechanical deformation, whereas the second term represents the reduction in pore volume associated with calcium carbonate precipitation.

$$\frac{\partial n}{\partial t} = (1-n)\frac{\partial}{\partial t}(\nabla \cdot \boldsymbol{u}) - \frac{(1-n)}{1-S_c}\frac{\partial S_c}{\partial t} \tag{15}$$

3.1.8 Stiffness

The increase in stiffness resulting from bio-cementation can be estimated using the empirical relationship proposed by [11]. By assuming a constant Poisson's ratio, the shear and bulk moduli may be expressed as functions of the degree of cementation through their relationship with Young's modulus, as given in Eqs. (16) and (17).

$$G = G_0\left(1 + \frac{9.7}{152} m_c C_c\right)^2 \tag{16}$$

$$K = K_0\left(1 + \frac{9.7}{152} m_c C_c\right)^2 \tag{17}$$

Here, G_0 and K_0 denote the initial shear and bulk moduli, whereas G and K represent the corresponding shear and bulk moduli of the cemented sample. C_c refers to the cement content.

3.1.9 Chemo-hydro-mechanical equilibrium

The elastic horizontal strain at any point in space and time can be expressed in terms of radial displacement within an elastic medium. By substituting Eq. (1) into the force balance equations, Eqs. (3) and (4), and rewriting the strain components in terms of displacement, Eqs. (18) and (19) are derived. These equations describe the coupled relationship among displacement, pore pressure, and calcium carbonate content.

$$\begin{aligned}&\frac{\partial}{\partial r}\left[\left(K + \frac{4G}{3}\right)\left(\frac{\partial u_r}{\partial r}\right) + \left(K - \frac{2G}{3}\right)\left(\frac{u_r}{r} + \frac{\partial u_z}{\partial z}\right)\right] + \\ &\frac{1}{r}\left[2G\left(\frac{\partial u_r}{\partial r} - \frac{u_r}{r}\right)\right] = \\ &\frac{\partial}{\partial r}\left[\alpha p + 3K\alpha_c m_c C_c\right]\end{aligned} \tag{18}$$

$$\begin{aligned}&\frac{\partial}{\partial z}\left[\left(K + \frac{4G}{3}\right)\left(\frac{\partial u_z}{\partial z}\right) + \left(K - \frac{2G}{3}\right)\left(\frac{u_r}{r} + \frac{\partial u_r}{\partial r}\right)\right] \\ &= \frac{\partial}{\partial z}\left[\alpha p + 3K\alpha_c m_c C_c\right] - \rho \boldsymbol{g}\end{aligned} \tag{19}$$

3.1.10 Chemical species transport equation

Because the reaction rate depends directly on urea concentration, it is necessary to solve the corresponding differential equation. The density-driven flow term is neglected, as its effect is minor compared with advection and dispersion. As a result, the governing equations for urea, dissolved calcium, and ammonium concentrations are derived in Eqs. (20) to (22).

$$\frac{\partial C_u}{\partial t} = -\left(\frac{\boldsymbol{q}}{n}\right)\nabla C_u + \nabla \cdot (\boldsymbol{D} \cdot \nabla C_u) - R_{react} \tag{20}$$

$$\frac{\partial C_{Ca}}{\partial t} = -\left(\frac{\boldsymbol{q}}{n}\right)\nabla C_{Ca} + \nabla \cdot (\boldsymbol{D} \cdot \nabla C_{Ca}) - R_{react} \tag{21}$$

$$\frac{\partial C_{NH_4^+}}{\partial t} = -\left(\frac{\boldsymbol{q}}{n}\right)\nabla C_{NH_4^+} + \nabla \cdot \left(\boldsymbol{D} \cdot \nabla C_{NH_4^+}\right) + 2R_{react} \tag{22}$$

Neglecting the effect of density-driven flow, the governing equation for calcium carbonate concentration can be obtained, as presented in Eq. (23). In this formulation, the first term on the right-hand side represents calcium carbonate precipitation induced by urea hydrolysis, while the second term captures the effect of porosity changes on calcium carbonate concentration.

$$\begin{aligned}\frac{\partial C_c}{\partial t} = &\left(\frac{n}{1-n}\right) R_{react} - \\ &\left(\frac{m_c}{\rho_c}\right)\left(\frac{n}{1-n}\right) R_{react} C_c\end{aligned} \tag{23}$$

Variations in porosity, represented by the fluid volume fraction n, directly affect the solid volume fraction $(1-n)$ and, consequently, influence the concentration of precipitated calcium carbonate when expressed relative to the solid phase volume.

3.1.11 Bacteria transport equation

By neglecting density-driven flow effects, the governing expression for the concentration of suspended bacteria can be written as given in Eq. (24).

$$\begin{aligned}\frac{\partial B_f}{\partial t} = &-\left(\frac{\boldsymbol{q}}{n}\right)\nabla B_f + \nabla \cdot \left(\boldsymbol{D} \cdot \nabla B_f\right) \\ &- R_{attach} B_f - R_{decay} B_f\end{aligned} \tag{24}$$

In this equation, the first term on the right-hand side represents the rate of bacterial attachment to the solid phase, whereas the second term accounts for the effect of porosity variation, n, on the concentration of adsorbed bacteria.

$$\begin{aligned}\frac{\partial B_s}{\partial t} = &\left(\frac{n}{1-n}\right) R_{attach} B_f - \\ &\left(\frac{m_c}{\rho_c}\right)\left(\frac{n}{1-n}\right) R_{react} B_s - R_{decay} B_s\end{aligned} \tag{25}$$

3.1.12 Flow equation

By incorporating the pressure-dependent behavior of fluid density through the definition of a compressibility coefficient, the mass balance equation for pore water can be reduced to the simplified form given in Eq. (26), which represents the general flow equation.

$$\frac{\partial n}{\partial t} = -\frac{n}{K_f}\frac{\partial \rho_f}{\partial t} - \nabla \cdot \left(n \boldsymbol{v_f}\right) \tag{26}$$

By formulating the grain mass balance and accounting for grain compressibility, the hydro-mechanical part of the model can be established. Variations in grain density are expressed as functions of stress and pore pressure. These relationships, combined with Darcy's law, changes in calcium carbonate content, and the time-dependent form of σ in terms of medium compressibility and pore pressure, yield the general fluid flow equation presented in Eq. (27).

$$\frac{k}{\mu}\nabla\cdot\left(\nabla p+\rho_f g\right)-\left(\frac{n}{K_f}+\frac{\alpha-n}{K_g}\right)\frac{\partial p}{\partial t}= \alpha\frac{\partial}{\partial t}(\nabla\cdot\boldsymbol{u})-n\frac{m_c}{\rho_c}R_{react} \quad (27)$$

3.2 Modeling framework

The model considers a one-dimensional soil column with a height of 14 cm and a diameter of 7.2 cm, representing a laboratory-scale bio-cementation treatment setup. The model input parameters are summarized in Table 1.

Table 1. Input parameters of the model.

Parameter(s)	Input	Parameter(s)	Input
K (MPa)	100	G (MPa)	75
K_f (GPa)	2	K_g (GPa)	80
ρ_g (kg/m^3)	2600	ρ_w (kg/m^3)	1000
α	1	α_c	10^{-5}
n_0	0.375	k_0 (m^2)	1.02×10^{-12}
μ (Pa.s)	0.001	q_{inj} (m/s)	2×10^{-5}
ρ_c (kg/m^3)	2710	m_c (kg/kmol)	100.1
D_{diff} (m^2/s)	2×10^{-9}	C_0 (kmol/m^3)	0.25
B_0 (OD)	1	K_m	0.001
u_b (kmol /m^3.sOD)	2×10^{-5}	t_{max} (s)	28800
K_{attach} (1/s)	3×10^{-4}		

The column is first saturated until reaching steady-state conditions. This was followed by 1 cycle of bacterial injection for 45 minutes, corresponding to 1 pore volume of the sample (PV), after which the system was kept closed for 6 hours to allow bacterial retention. A cementation solution was then introduced for 45 minutes in each cycle, equivalent to 1 PV per cycle, followed by a 6-hour retention period to enable the reaction between the injected solution and the bacteria present in the medium. To investigate the effect of cyclic treatment, four different cementation scenarios consisting of 3, 4, 5, and 8 cycles were considered.

4 Model verification

To reproduce the MICP treatment conditions reported by Fauriel and Laloui [7], the characteristic parameters and boundary conditions from their study were adopted. The column height and diameter were assigned according to the geometry reported by Fauriel and Laloui [7], as shown in Fig. 1. Four points along the height of the column were selected to be able to compare and verify the results of the FE model against Fauriel and Laloui [7]. The result of the verification of the precipitated calcium carbonate is presented in Fig. 2.

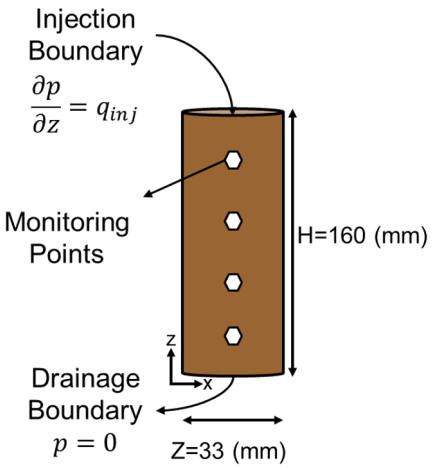

Fig. 1. Schematic of the geometry and boundary conditions.

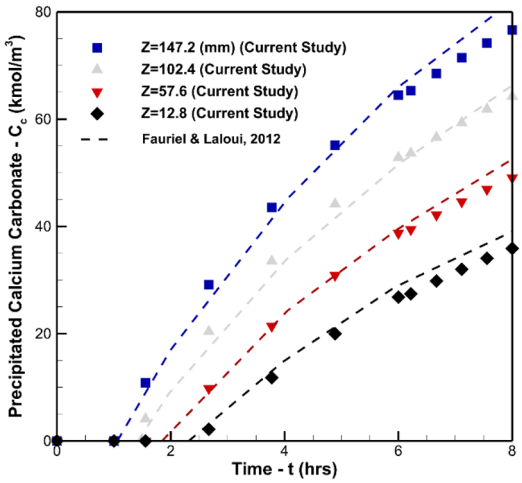

Fig. 2. Verification of the coupled BCHM model against Fauriel & Laloui [7].

5 Results

This section presents the results of calcium carbonate precipitation under different treatment scenarios. The results are reported both in terms of injected volume of cementation solution and bio-cement content (CC%) along the column height to enable comparison with cement content measurements obtained from laboratory testing. The precipitated $CaCO_3$ results are reported at the end of each retention cycle to reflect the progress of cementation with increase in the volume of cementation solution during the treatment. As shown in Fig. 3, for the first scenario, in which 3 cycles of cementation solution were injected, the maximum CC% at the end of three cycles reached 2.1% at the injection point, while the difference between the nearest and farthest monitoring locations was approximately 1.4%. For the case of 4 cycles cementation injection, the maximum CC% increased to 2.7%, with a spatial difference of less than 2%. When 5 cycles of cementation solution were

applied, the maximum CC% further increased to 3.4%, and the difference between the injection point and the monitoring location at 10.1 cm reached 2.2%. As anticipated, the highest precipitation was obtained for the 8 cycles scenario, where the maximum CC% reached 5%, with a difference of 3% across the column. Increasing the injected cementation solution volume from 3 to 4 cycles produces an approximately 27% increase in CC% along the column. This increase reaches about 55% when the injected volume is raised from 3 to 5 cycles, while increasing the volume from 3 to 8 cycles nearly doubles the amount of precipitated bio-cement.

Using the difference in precipitated $CaCO_3$ between the monitoring point closest to the injection location and the farthest monitoring point as an indicator of spatial non-uniformity, the degree of non-uniformity increased from approximately 1.35% in the 3 cycles case to 1.75%, 2.05%, and 3.00% in the 4, 5, and 8 cycles cases, respectively. Relative to the 3 cycles condition, these values represent increases of about 30%, 52%, and 122%, demonstrating that higher cementation solution volumes lead to progressively greater heterogeneity in calcium carbonate distribution.

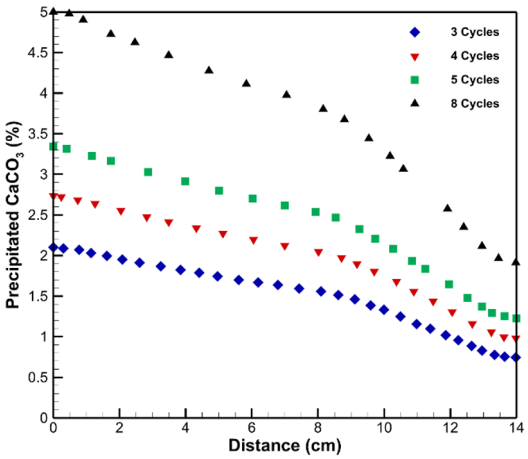

Fig. 3. Effect of cementation solution injection cycles on precipitated $\boldsymbol{CaCO_3}$ along the column height.

Fig. 4 presents the contours of urea concentration and precipitated $CaCO_3$ after 8 cycles of cementation-solution injection. As shown in Fig. 4a, the urea concentration is not uniformly distributed along the column height. Lower urea concentrations are observed near the bottom of the column, while higher concentrations remain toward the upper region. This trend suggests greater urea consumption in the lower portion of the specimen, which may be associated with more active ureolysis and reactant utilization in that region. The gradual increase in residual urea concentration toward the top indicates that urea was not fully consumed throughout the column, reflecting the coupled effects of reactant transport, bacterial distribution, and reaction kinetics.

The corresponding $CaCO_3$ distribution is shown in Fig. 4b. Similar to the urea profile, the precipitated calcium carbonate exhibits a clear vertical gradient, with lower accumulation near the bottom and higher accumulation toward the top of the column. This indicates that although 8 cementation cycles promoted substantial bio-cement production, the precipitation remained spatially non-uniform. The higher $CaCO_3$ content in the upper region may be related to greater local reactant availability and more favorable precipitation conditions, while the lower values near the bottom may result from reactant depletion, limited bacterial retention, or changes in flow behavior caused by progressive pore filling.

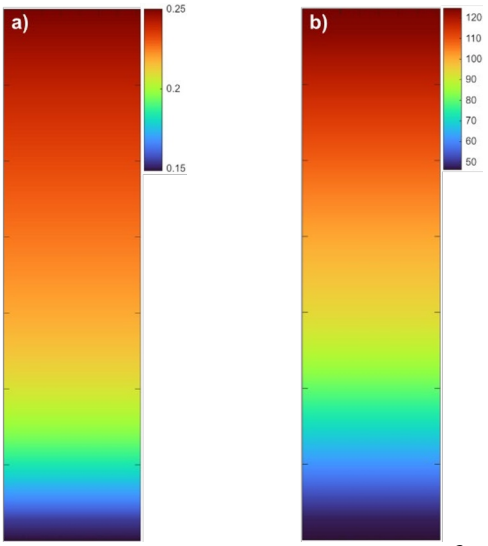

Fig. 4. Contours of: a) urea concentration ($\mathbf{kmol/m^3}$) and b) precipitated $\boldsymbol{CaCO_3}$ ($\mathbf{kg/m^3}$) after 8 cycles of cementation solution injection.

Although the trend in Fig. 5 confirms that greater injection volumes enhance calcium carbonate precipitation, excessive injections may also induce clogging near the injection boundary. Moreover, non-uniform bio-cementation decreases the efficiency with which precipitated $CaCO_3$ contributes to strength gain [12]. As a result, a more uniform and contact-effective distribution of bio-cement is likely to yield higher unconfined compressive strength (UCS) than a more localized, heterogeneous precipitation pattern caused by clogging [12].

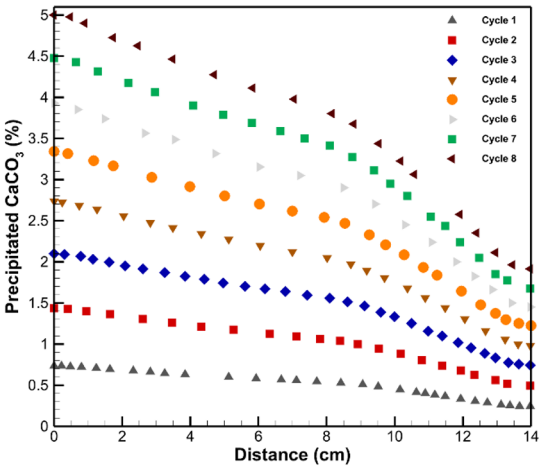

Fig. 5. Precipitated $\boldsymbol{CaCO_3}$ along the column for 3, 4, 5, and 8 cycles of cementation solution injection.

6 Conclusions

This study carried out a detailed parametric investigation using a coupled bio-chemo-hydro-mechanical model to examine the influence of the volume of the cementation solution being injected into the treated sand on bio-cementation. The results demonstrate that increasing the number of cementation injection cycles enhances calcium carbonate precipitation throughout the column. Nevertheless, the spatial variability of CC% becomes more pronounced at higher injection volumes, suggesting that while additional cementation cycles improve the overall degree of bio-cementation, they may also produce a more heterogeneous precipitation distribution along the sample. These results provide a useful benchmark for optimizing cyclic MICP treatment strategies at the laboratory scale and offer guidance for future scale-up studies.

References

1. J. T. DeJong, M. B. Fritzges, and K. Nüsslein, Microbially induced cementation to control sand response to undrained shear, J. Geotech. Geoenviron. Eng., **132**(11), pp. 1381–1392, (2006).
2. J. K. Mitchell and J. C. Santamarina, Biological considerations in J. Geotech. Geoenviron. Eng., **131**(10), pp. 1222–1233, (2005).
3. M. G. Gomez, J. T. DeJong, and C. M. Anderson, Effect of bio-cementation on geophysical and cone penetration measurements in sands, Can. Geotech. J., **55**(11), 1632–1646, (2018).
4. A. Nafisi, D. Mocelin, B. M. Montoya, and S. Underwood, Tensile strength of sands treated with microbially induced carbonate precipitation, Can. Geotech. J., **57**(10), 1611–1616, (2020).
5. R. Mehrabi and K. Atefi-Monfared, A coupled bio-chemo-hydro-mechanical model for bio-cementation in porous media, Can. Geotech. J., **59**(7), 1266–1280, (2022).
6. T. Barkouki et al., Forward and inverse bio-geochemical modeling of microbially induced calcite precipitation in half-meter column experiments, Transp. Porous Media, **90**(1), 23–39, 2011.
7. S. Fauriel and L. Laloui, A bio-chemo-hydro-mechanical model for microbially induced calcite precipitation in soils, Comput. Geotech., **46**, 104–120, 2012.
8. W. Van Wijngaarden, F. Vermolen, G. Van Meurs, and C. Vuik, Modelling biogrout: a new ground improvement method based on microbial-induced carbonate precipitation, Transp. Porous Media, **87**(2), pp. 397–420, 2011.
9. W. Van Wijngaarden, F. Vermolen, G. Van Meurs, and C. Vuik, A mathematical model for biogrout: bacterial placement and soil reinforcement, Comput. Geosci., **17**(3), 463–478, 2013.
10. X. Wang and U. Nackenhorst, A coupled bio-chemo-hydraulic model to predict porosity and permeability reduction during microbially induced calcite precipitation, Adv. Water Resour., **140**, 103563, 2020.
11. L. A. van Paassen, R. Ghose, T. J. van der Linden, W. R. van der Star, and M. C. van Loosdrecht, Quantifying biomediated ground improvement by ureolysis: large-scale biogrout experiment, J. Geotech. Geoenviron. Eng., **136**(12), 1721–1728, 2010.
12. R. Mehrabi and K. Atefi-Monfared, Comparative analysis of silt, kaolinite, and montmorillonite particle effects on bio-cementation in sandy soils, Can. Geotech. J., **62**, pp. 1–18, 2025.